ACS OMEGA

http://pubs.acs.org/journal/acsodf

Article

First-Principles Investigations of Thermoelectric Behavior of RuCrX (X = Si, Ge, Sn)

Muhammad Asif, Ayash O Alrashdi, Mohammed M. Fadhali, A. Afaq, and Abu Bakar*

Cite This: *ACS Omega* 2022, 7, 45353−45360

Read Online

ACCESS | Metrics & More | Article Recommendations

ABSTRACT: The half-Heusler alloys have not only been recognized for spintronic and memory devices but also for thermoelectric applications. In this research work, the detailed study for thermoelectric parameters of RuCrX (X = Si, Ge, Sn) half-Heusler alloys has been carried out by using the pseudopotential approach alongside the Boltzmann transport theory. The RuCrX (X= Si, Ge, Sn) was reported stable in $C1_b$-type structure by means of energy-volume optimization, elastic stability criteria, positive phonon frequencies in phonon dispersion curves, and formation energies. The all important thermoelectric properties of these alloys have not yet been explored. The thermoelectric properties such as Seebeck coefficient, electronic part of thermal conductivity, electrical conductivity, and power factor have been discussed within a specific temperature range (300−1200 K). The calculated value of the power factor was found to be 5.11 × 10^{11} W/(m K^2 s) for RuCrSi, 3.42 × 10^{11} W/(m K^2 s) for RuCrGe, and 1.85 × 10^{11} W/(m K^2 s) for RuCrSn at 1200 K.

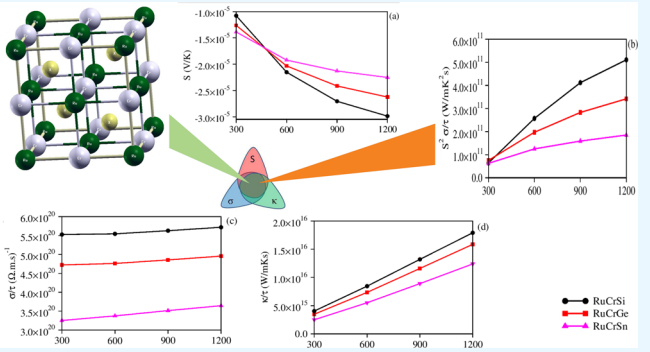

INTRODUCTION

The increasing energy crisis is a point of concern for humans. The two principle sources of renewable energy which can counteract this problem are waste heat converted into electrical energy and solar energy.[1,2] Continuous efforts have been made in the past, and it is still the topic of interest for the material scientists to find such imperative thermoelectric materials for power generation and alternative sources of energies with low toxicity and high Seebeck coefficient that are cost-effective and easy to synthesize.[3,4] To overcome these requirements, Gajaria and his co-workers attempted to find suitable materials with better thermoelectric performance.[5,6] They studied gallium- and carbon-based pnictides GaX (X = P, As, Sb) and α-CX (X = N, P). They predicted that GaSb is more efficient for thermoelectric applications with an overall figure of merit of 0.72 in a cubic ZB-structure at 1200 K. This was further supported by thermal conductivity. Sattigeri et al. studied the effect of band inversion on thermoelectric performance of gold iodide.[7] Remarkable thermal transport properties were observed due to significant coupling between the phonon modes, and the overall figure of merit for electrons and holes was found to be 0.58 and 0.57, respectively, at 300 K. The high temperature improved performance of dual-doped nontoxic $Ca_3Co_4O_9$ was predicted recently.[8] The hole-doped GeSe materials have been predicted to exhibit extraordinary thermoelectric performance owing largely to extremely low thermal conductivity.[9] Developing novel materials composed of earth abundant and nontoxic elements will aid progress toward the goal of sustainable thermoelectric materials. Dwivedi et al.[10] chemically synthesized CuZnSnS nanocrystals and fabricated a Cu_3ZnSnS_{5-y} thermoelectric material using nanocrystals as building blocks. The figure-of-merit (ZT) value of the Cu_3ZnSnS_{5-y} material was found to be 0.39 at 658 K. A theoretical attempt had been made by Paudel and Tsymbal[11] to find sizable values of the key thermoelectric parameters, such as the maximum power factor PF = 928 μW K^{-2} and the maximum figure of merit ZT = 0.48 for an electron-doped sample and PF = 74 μW K^{-2} and ZT = 0.17 for a hole-doped sample at room temperature, and a small doping level of ±0.25e per unit cell. The increase in temperature yields an increase in both the power factor and the figure of merit, reaching large values of PF = 3078 μW K^{-2} and ZT = 0.77 for the electron-doped sample and PF = 650 μW K^{-2} and ZT = 0.62 for the hole-doped sample at 800 K. The effect of doping on the thermoelectric performance of FeAsS had been studied theoretically by Zhu and his co-workers,[12] and it was found that p-type doping has better thermoelectric performance than n-type doping.

Received: September 13, 2022
Accepted: November 18, 2022
Published: December 2, 2022

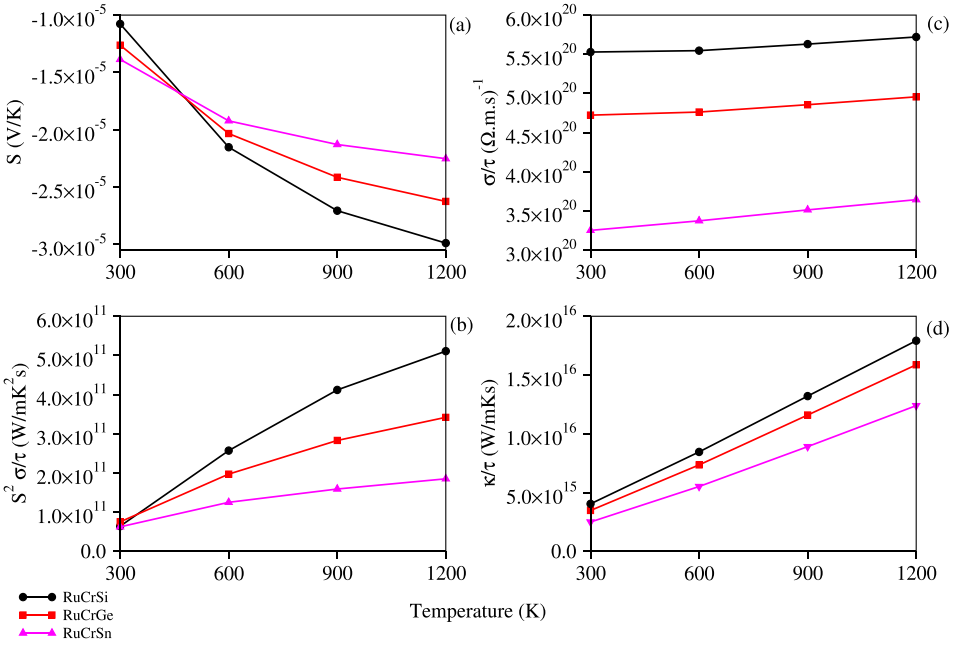

Figure 1. Variation of (a) Seebeck coefficient, (b) power factor, (c) electrical conductivity, (d) thermal conductivity of RuCrX (X = Si, Ge, Sn) against temperature.

Heusler alloys were discovered at the end of the 19th century but remained for many years a scientific curiosity because of their fascinating ferromagnetism, being composed of nonferromagnetic elements. There are only four ferromagnetic elements: Fe, Co, Ni, and Gd. The number of papers published on Heusler alloys is over 6000,[13] but the majority occurred after the significant discovery of their half metallicity (having both metallic and semiconductor character) in 1983 by de Groot.[14] This property makes them excellent candidates for spintronic devices, which were made possible by the discovery of the giant magnetoresistance (GMR) effect in 1988. The multifunctional application range of half-Heusler alloys has attracted researchers. Apart from the magnetic device applications, the alloys are equally useful in the field of thermoelectric devices[15] and generators with high Seebeck coefficient,[16−18] topological insulators,[19] and piezoelectric semiconductors.[20] Significant interest in these compounds stems from magnetism and the strong coupling of magnetism to strain, structural transitions, and band topology.[21] The general formula for half-Heusler alloys is XYZ where both X and Y belongs to metal family while Z is an element of nonmetallic nature. The half-Heuslers have $F\bar{4}3m$ space group and $C1_b$-type structure with potential applications due to the diverse physical properties.[22] A series of attempts have been made to check the thermoelectric response of half-Heuslers by different renowned groups. Manoj and Sanyal studied the lithium and magnesium based half-Heusler alloys and predicted the large values of Seebeck coefficient and power factors akin to a well-known thermoelectric material PbTe.[23] Tahir and Gupta worked on CrTiSi half-Heusler alloy, and a high power factor of 1.2 × 10^{12}W/(m K^2 s) at 800 K was predicted.[24] This motivates us to check the thermoelectric performance of RuCrX (X = Si, Ge, Sn) alloys. These alloys were first investigated for reststrahlen band calculations by Afaq et al.[25] by using the well-known pseudopotentials approach within the PBE-GGA. They concluded the stability with structural position Ru at (0.5, 0.5, 0.5), Cr at (0, 0, 0), and X at (0.25, 0.25, 0.25). The positive phonon frequency criteria[26−28] was also exploited to prove these alloys stable. They further proved these alloys stable by means of the elastic, mechanical, and reststrahlenband of these alloys for far-infrared and terahertz technology.[25,29] Interestingly these alloys are motivational in themselves as these are the Heusler alloys other than the combination of transition and rare earth metals.

METHOD AND COMPUTATIONAL APPROACH

We used here the density functional theory, which is one of the most accurate theories to calculate the electronic structure of solid materials. This technique is increasingly used as an exploratory tool for material discovery and in computational experiments.[30] The ability to predict structure−property relationships has revolutionized experimental fields, such as vibrational and solid-state NMR spectroscopy. In semiconductor physics, great progress has been made in the electronic structure of bulk and defect states despite the severe challenges presented by the description of excited states.[31,32] The thermoelectric parameters calculations were done by solution of Boltzmann transport equations. These calculations were carried out by using norm-conserving Troullier-Martins pseudopotentials within Perdew Burke Ernzerhof Generalized Gradient Approximations[33] for the recovery of exchange correlation energy with plane-wave basis as implemented in Quantum ESPRESSO.[34] The kinetic cutoff energy for wave function and charge density was set to have a value 50 and 400 Ry, respectively, for all alloys under study. The k-mesh sampling for irreducible Brillouin zone (IBZ) integration was performed with a Monkhorst Pack[35] mesh of 12 × 12 × 12 for self-consistent calculations and 24 × 24 × 24 for non-self-consistent calculations. The threshold for convergence was set to be extensive rather than the default one. The transport calculations were performed by the BoltzTrap[36] code. For power factor ($S^2\sigma/\tau$) calculations, the values of electrical conductivity and Seebeck coefficient are required. These two

https://doi.org/10.1021/acsomega.2c05928
ACS Omega 2022, 7, 45353−45360

quantities appear as a function of chemical potentials and temperature as

$$\sigma_{\alpha\beta}(T, \mu) = \frac{1}{\Omega}\int \sigma_{\alpha\beta}(\epsilon)\left[-\frac{\partial f_o(T, \epsilon, \mu)}{\partial \epsilon}\right] d\epsilon \quad (1)$$

$$S_{\alpha\beta}(T, \mu) = \frac{1}{eT\Omega\sigma_{\alpha\beta}(T, \mu)}\int \sigma_{\alpha\beta}(\epsilon)(\epsilon - \mu)\left[-\frac{\partial f_o(T, \epsilon, \mu)}{\partial \epsilon}\right] d\epsilon \quad (2)$$

the unit cell volume is Ω, the Fermi−Dirac distribution is f_o, and the electronic charge is e.

$$\sigma_{\alpha\beta}(\epsilon) = \frac{e^2}{N}\sum_{i,k}\tau_{i,\mathbf{k}}\nu_\alpha(i, \mathbf{k})\nu_\beta(i, \mathbf{k})\frac{\delta(\epsilon - \epsilon_{i,\mathbf{k}})}{d\epsilon} \quad (3)$$

In eq 3, k points are represented by N and band index i. Wave vector $\mathbf{k}$ and group velocity $\nu_\alpha(i, \mathbf{k})$ can be obtained from electronic dispersion relations.

$$\nu_\alpha(i, \mathbf{k}) = \frac{1}{\hbar}\frac{\partial \epsilon_{i,\mathbf{k}}}{\partial k_\alpha} \quad (4)$$

$\hbar$ is the reduced Planck's constant in eq 4.

RESULTS AND DISCUSSIONS

Thermoelectric Properties. Thermoelectric devices are often regarded as the alternate energy source as waste heat is converted into useful electrical energy. So, in this section we present the various transport properties such as Seebeck coefficient (S), electrical conductivity (σ/τ), electronic part of thermal conductivity (κ_e/τ), and power factor (PF). Some additional parameters like specific heat capacity (C_v), Hall coefficient (R_H), susceptibility (χ), and charge carrier densities are also checked. A large number of half-Heusler materials have been reported for thermoelectric applications but the majority of those reported materials have positive Seebeck coefficients which means the majority of the carriers are holes. In this current research work the Seebeck coefficient is negative which means the majority carriers are electrons. The next important difference from already reported materials is in the behavior in density of states at valence band maxima and conduction band minima. The already reported materials do have a high density of states at band edges especially at valence band maxima while in this current research work the materials under study have the high density of states both at valence band maxima and conduction band minima.[29] This peculiarity yields the negative Seebeck coefficient and makes these compounds superior than other ones. These Heusler alloys are attractive as they are other than the combination of transition and rare earth metals. In general, for better thermoelectric efficiency the value of the Seebeck coefficient just inside the band edge is important, and the material retains considerable value of the Seebeck coefficient. In Figure 1, the change of the Seebeck coefficient, power factor, thermal conductivity, and electrical conductivity is presented with increasing temperature for all these materials. The Seebeck coefficient is a function of density of states of a material, and its commonly used form is derived from the Boltzmann transport equation and described as

$$S = \frac{k_B}{e}\left[\left(\frac{E_F - E_{\text{Trans}}}{k_B T}\right) - A\right] \quad (5)$$

where A is the heat of transport. However, the Fermi energy along with the transport energy varies in a very systematic way, mentioned in Table 1, clearly depicting the relevance.

The estimated values of the Seebeck coefficient at different temperatures are calculated and tabulated in Table 2. It is clear from these listed results that the Seebeck coefficient changes from -1.07×10^{-3} V/K to -2.98×10^{-3} V/K for RuCrSi; -1.26×10^{-3} V/K to -2.62×10^{-3} V/K for RuCrGe and -1.38×10^{-3} V/K to -2.25×10^{-3} V/K for RuCrSn when the temperature is changed from 300 K to 1200 K. The variation against the potential is also interesting in that it decreases first

Table 1. Fermi Energy and Transport Energy for RuCrX (X= Si, Ge, Sn)

Material	E_F (eV)	E_{Trans} (eV)
RuCrSi	11.4140	11.4138
RuCrGe	10.8653	10.8641
RuCrSn	9.8906	9.8899

Table 2. Seebeck Coefficient in Unit V/K, Power Factor in Unit W/(m K^2 s), electrical conductivity in unit $(\Omega\cdot m\cdot s)^{-1}$ and thermal conductivity in unit W/(m K s) for RuCrX (X = Si, Ge, Sn) at Various Temperatures

parameter	300 K	600 K	900 K	1200K
		Alloy = RuCrSi		
Seebeck	-1.07×10^{-3}	-2.15×10^{-3}	-2.70×10^{-3}	-2.98×10^{-3}
$S^2\sigma/\tau$	6.41×10^{10}	2.57×10^{11}	4.12×10^{11}	5.11×10^{11}
σ/τ	5.52×10^{22}	5.54×10^{22}	5.62×10^{22}	5.72×10^{22}
κ_e/τ	4.03×10^{17}	8.45×10^{17}	1.32×10^{18}	1.79×10^{18}
		Alloy = RuCrGe		
Seebeck	-1.26×10^{-3}	-2.03×10^{-3}	-2.41×10^{-3}	-2.62×10^{-3}
$S^2\sigma/\tau$	7.52×10^{10}	1.97×10^{11}	2.83×10^{11}	3.42×10^{11}
σ/τ	4.72×10^{22}	4.76×10^{22}	4.85×10^{22}	4.95×10^{22}
κ_e/τ	3.47×10^{17}	7.35×10^{17}	1.15×10^{18}	1.58×10^{18}
		Alloy = RuCrSn		
Seebeck	-1.38×10^{-3}	-1.92×10^{-3}	-2.12×10^{-3}	-2.25×10^{-3}
$S^2\sigma/\tau$	6.52×10^{10}	1.25×10^{11}	1.59×10^{11}	1.85×10^{11}
σ/τ	3.25×10^{22}	3.37×10^{22}	3.51×10^{22}	3.64×10^{22}
κ_e/τ	2.49×10^{17}	5.51×10^{17}	8.90×10^{17}	1.23×10^{18}

https://doi.org/10.1021/acsomega.2c05928
ACS Omega 2022, 7, 45353−45360

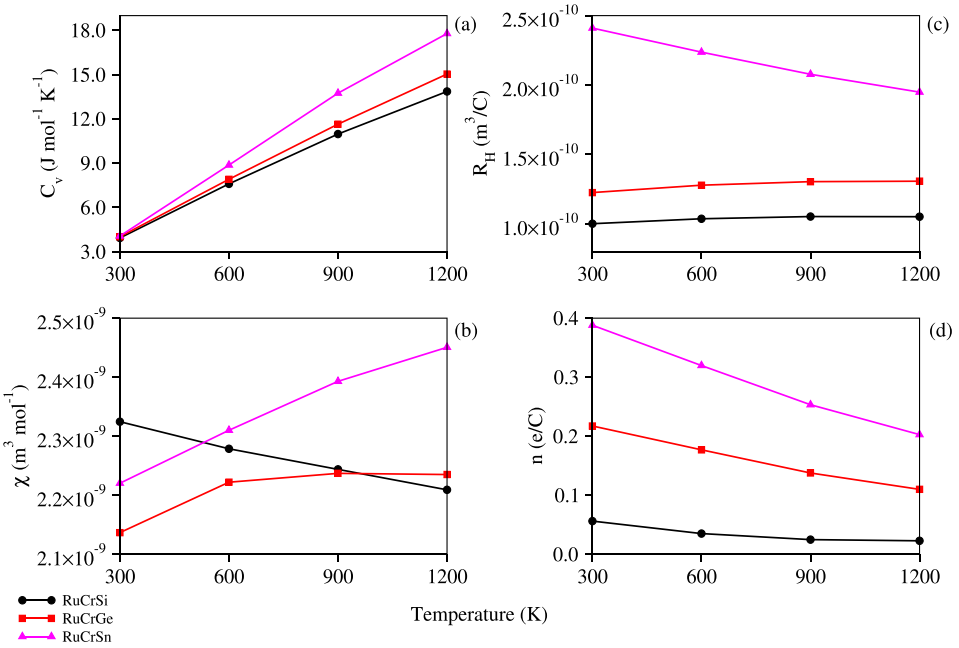

Figure 2. Variation of (a) specific heat capacity at constant volume; (b) susceptibility; (c) Hall coefficient. (d) The charge carrier densities of RuCrX (X = Si, Ge, Sn) against temperature.

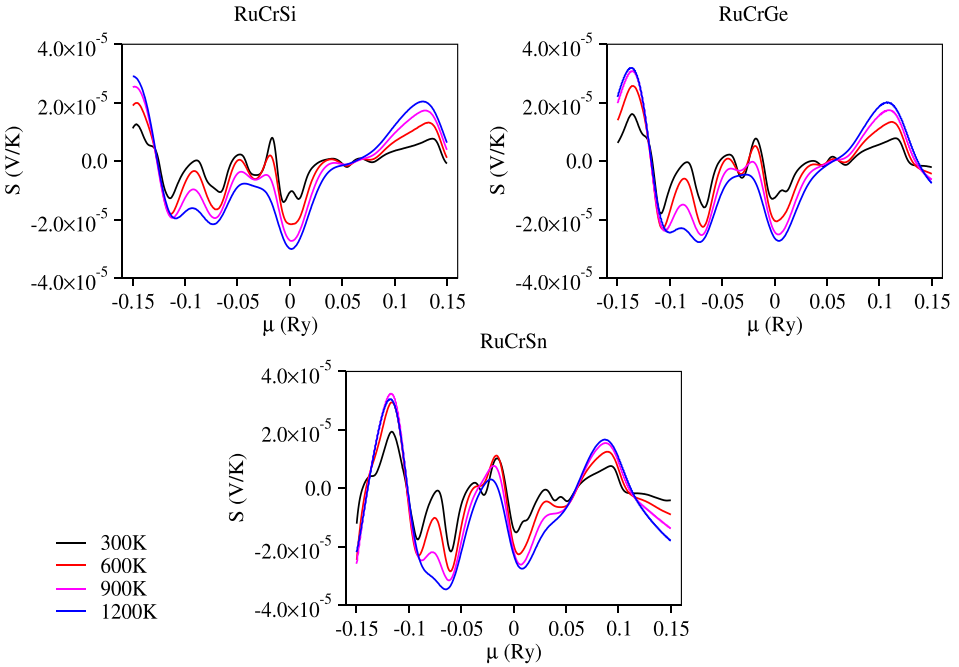

Figure 3. Variation of Seebeck coefficient of RuCrX (X = Si, Ge, Sn) against potential.

and then converges near the Fermi energy and increases afterward (see Figures 1a and3).

The change in the electrical conductivity (σ/τ) is small when temperature changes from 300 K to 1200 K and RuCrSi has the highest value which is also clear from Figures 1c and 4. The estimated values are tabled (see Table 2). The thermal conductivity of a solid material is completely discussed in terms of the lattice thermal conductivity (κ_l) and electronic thermal conductivity (κ_e). Here the electronic part of the thermal conductivity is studied with its variation against temperature as well as the potentials and shown in Figure 1d and Figure 5. The thermoelectric parameters are coupled with the relaxation time, and this relation is well explained by Saini et al.[37] The transport properties of thermoelectric materials are usually calculated using the semiclassical Boltzmann transport theory within constant relaxation time (τ) approximation.[36,38] Within this constant τ approximation, calculated values of σ and κ_e depend linearly on τ. The temperature dependence of τ is usually ignored while calculating thermoelectric properties.[39−42] As far as the ratio σ/κ_e is concerned for efficiency, the temperature dependence of τ is canceled. The computed values of thermal conductivity show the increasing trend for all alloys in the temperature interval 300 K to 1200 K.

https://doi.org/10.1021/acsomega.2c05928
ACS Omega 2022, 7, 45353−45360

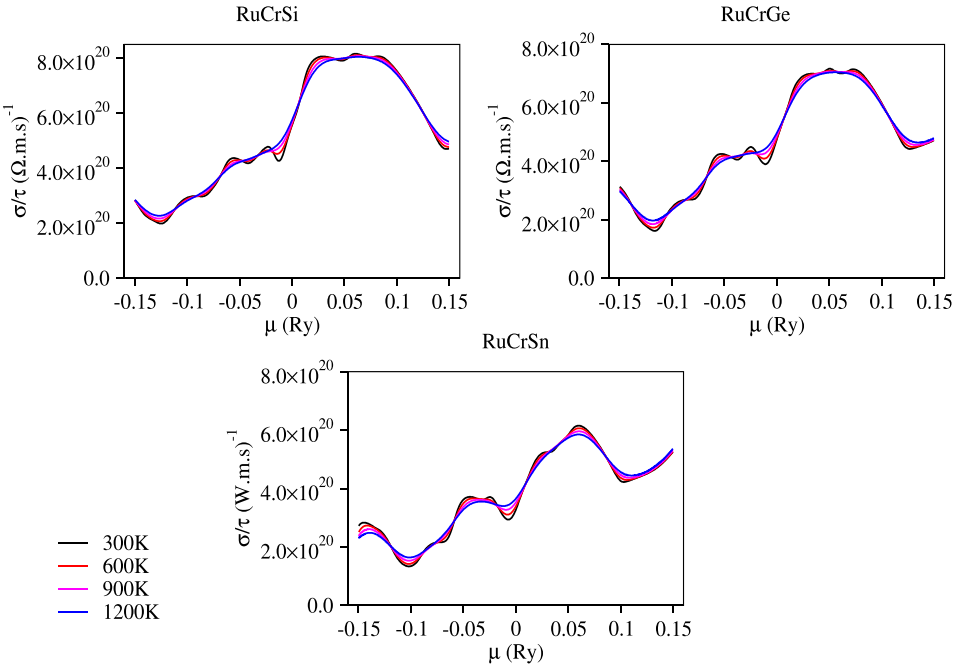

Figure 4. Variation of electrical conductivity of RuCrX (X = Si, Ge, Sn) against potential.

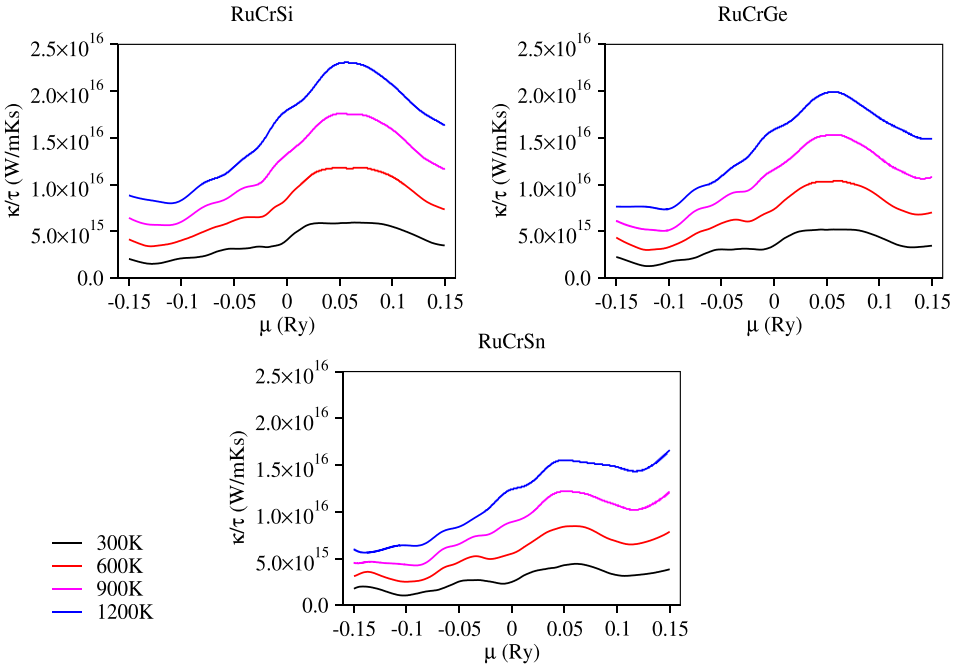

Figure 5. Variation of thermal conductivity of RuCrX (X = Si, Ge, Sn) against potential.

It can bee seen from Figure 1b that the power factor (PF) of RuCrX (X = Si, Ge, Sn) alloys is increasing. It is very interesting to note that PF is varying almost linearly for these alloys, and this variation is greater as the temperature reaches 1200 K which make them even more interesting as application prospectives. It is increasing from 6.41×10^{10} W/(m K^2 s) to 5.11×10^{11} W/(m K^2 s) for RuCrSi; 7.52×10^{10} W/(m K^2 s) to 3.42×10^{11} W/(m K^2 s) for RuCrGe; 6.52×10^{10} W/(m K^2 s) to 1.85×10^{11} W/(m K^2 s) for RuCrSn at 300 K to 1200 K. So there is a valuable increase in the power factor for RuCrX (X = Si, Ge, Sn) being that it is a thermoelectric material. Similar trends and results were predicted by Uzma et al.[8]

Beside these thermoelectric parameters, the thermodynamic response such as specific heat capacity at constant volumes (C_v), Hall coefficient (R_H), susceptibility (χ) better known as thermal expansion coefficient, and charge carrier density (n) of these alloys against temperature (up to 1200 K) and potential are shown in Figures 2a–d and 6a–d. The capacity of any material to absorb heat is checked by the specific heat capacity (C_v) at constant volumes for harmonic approximation (HA). This factor is generally an effect of electronic heat capacity plus the effect of phonons in semiconductor materials. The increase in value is linear with the increase in temperature, and the value increases to 13.80, 15.03, and 17.78 for RuCrSi, RuCrGe,

https://doi.org/10.1021/acsomega.2c05928
ACS Omega 2022, 7, 45353−45360

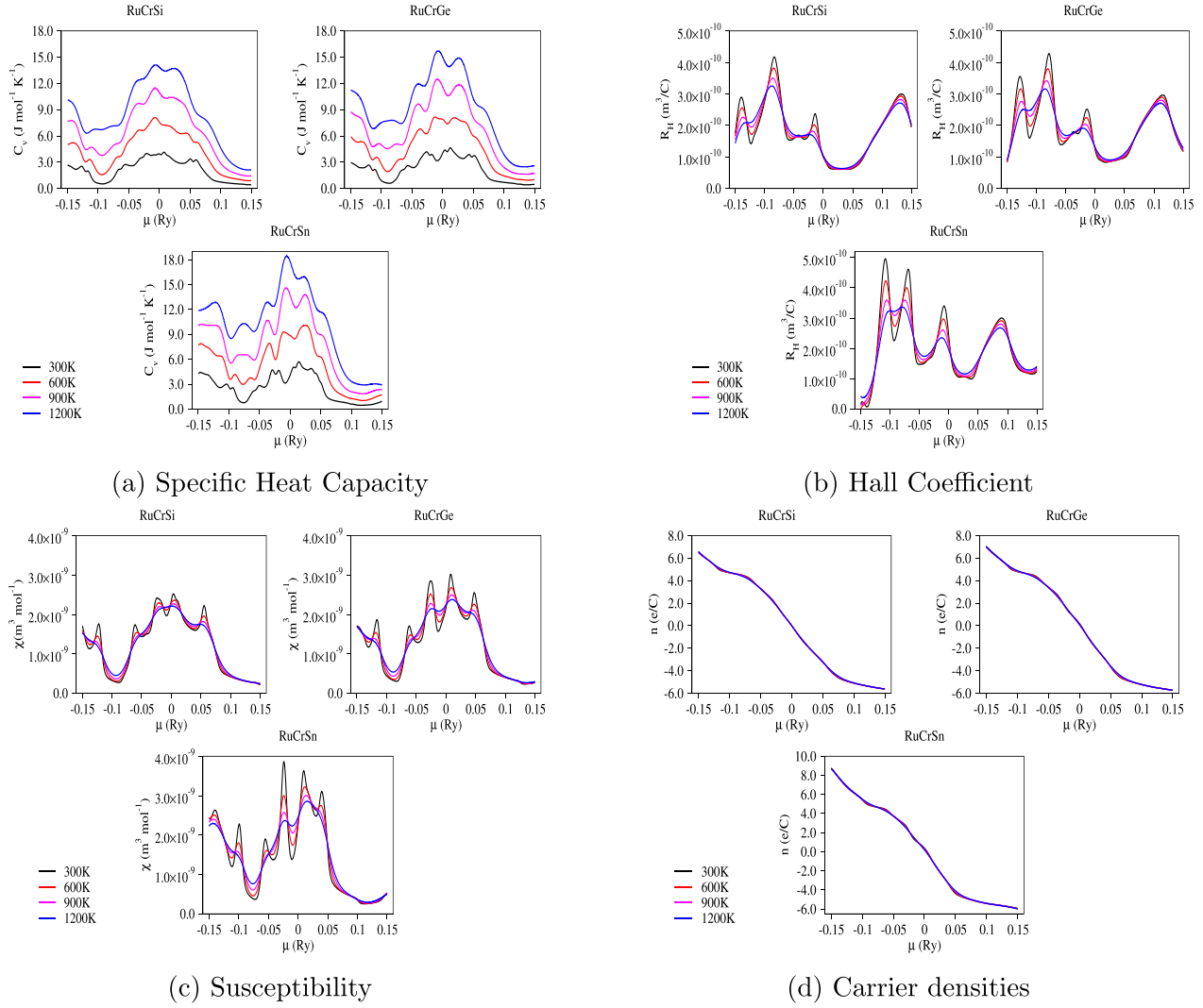

Figure 6. Variation of (a) specific heat capacity; (b) susceptibility; (c) Hall coefficient; and (d) charge carrier densities of RuCrX (X = Si, Ge, Sn) alloys.

RuCrSn at 1200 K, respectively (see Figure 2a). The Dulong-Petit law is followed by this increasing trend which concludes that C_v does not expand with the classical limit ∼3R, R being the gas constant. This linear increase shows that the Debye temperature rule is followed by molar heat capacity at lower temperature as well as T^3 law.[43] The Hall coefficient is shown in Figure 2c for different temperatures, and calculations show that R_H has mixed trends with changing temperature; e.g., at room temperature, RuCrSi and RuCrGe show the increase while RuCrSn shows a decrease and finally reaches to 1.94 × 10^{-10} m^3/C. The stable electric field is described by the Hall effect when opposite charge densities are accommodated at both ends of the semiconductor. This can further be supported by the fact that phonon vibrations increased when temperature is increased and as a result more scattering is observed in the materials.[44] The susceptibility (χ) of these materials is plotted against temperature (from 300 K to 1200 K), and potentials are shown in Figure 2b. This electrical response is in good agreement with the response of material checked in ref 45. Finally, Figure 2d clearly shows that the concentration of charge carriers (n) is decreasing with increasing temperature. The discussion of thermodynamics and thermoelectric parameters reveals the high value of specific heat capacity and thermal efficiency which favors the argument that these alloys are potential candidates for thermoelectric generators.

CONCLUSION

Thermoelectric response of half-Heuslers RuCrX (X = Si, Ge, Sn) having FCC structure has been investigated by using the pseudopotential approach alongside the Boltzmann transport theory. Thermoelectric response is checked by parameters such as Seebeck coefficient, electronic thermal conductivity, electrical conductivity, and power factor within a temperature range (300−1200 K). These materials have high Seebeck coefficient at room temperature with a value of −1.07 × 10^{-3} V/K for RuCrSi, −1.26 × 10^{-3} V/K for RuCrGe, and −1.38 × 10^{-3} V/K for RuCrSn. The negative value of the Seebeck coefficient over the entire temperature range suggests that the materials are n-type. The total thermal conductivity increases with increase in temperature. Furthermore, RuCrSi reaches a high PF of 5.11 × 10^{11} W/(m K^2 s) at 1200 K. The values of power factors and other thermoelectric parameters prove the suitability of these alloys for thermoelectric generators.

https://doi.org/10.1021/acsomega.2c05928
ACS Omega 2022, 7, 45353−45360

AUTHOR INFORMATION

Corresponding Author

Abu Bakar − *Centre of Excellence in Solid State Physics, University of the Punjab, Lahore 54000, Pakistan;* orcid.org/0000-0002-4647-0257; Email: abubakar.phd.cssp@pu.edu.pk

Authors

Muhammad Asif − *Department of Physics, COMSATS University Islamabad, Lahore 54000, Pakistan*

Ayash O Alrashdi − *King Abdulaziz City for Science and Technology, Riyadh 11442, Saudi Arabia*

Mohammed M. Fadhali − *Department of Physics, Faculty of Science, Jazan University, Jazan 45142, Saudi Arabia; Department of Physics, Faculty of Science, Ibb University, Ibb 70270, Yemen*

A. Afaq − *Centre of Excellence in Solid State Physics, University of the Punjab, Lahore 54000, Pakistan*

Complete contact information is available at: https://pubs.acs.org/10.1021/acsomega.2c05928

Notes

The authors declare no competing financial interest.

ACKNOWLEDGMENTS

The authors would like to express their sincere gratitude to respected reviewers who spared their time to review this manuscript meticulously and provided us with constructive comments. The role of respected editor is appreciated for the editorial feedback and handling. This work was not funded by any research grant and partially supported by the principal author Muhammad Asif.

REFERENCES

(1) Sajjad, M.; Mahmood, Q.; Singh, N.; Larsson, J. A. Ultralow Lattice Thermal Conductivity in Double Perovskite Cs_2PtI_6: A Promising Thermoelectric Material. *ACS Appl. Energy Mater.* **2020**, *3*, 11293−11299.

(2) Mahmood, Q.; e Hani, U.; Al-Muhimeed, T. I.; AlObaid, A. A.; Haq, B. U.; Murtaza, G.; Flemban, T. H.; Althib, H. Study of optical and thermoelectric properties of $ZYbI_3$ (Z. = Rb, Cs) for solar cells and renewable energy; Modelling by density functional theory. *J. Phys. Chem. Solids* **2021**, *155*, 110117−110123.

(3) Chai, Y. W.; Oniki, T.; Kimura, Y. Microstructure and thermoelectric properties of a $ZrNi_{1.1}Sn$ half-Heusler alloy. *Acta. Mater.* **2015**, *85*, 290−300.

(4) Kim, S. W.; Kimura, Y.; Mishima, Y. High temperature thermoelectric properties of TiNiSn-based half-Heusler compounds. *Intermetallics* **2007**, *15*, 349−356.

(5) Gajaria, T. K.; Dabhi, S. D.; Jha, P. K. ab initio energetics and Thermoelectric Profles of Gallium pnictide polytypes. *Sci. Rep.* **2019**, *9* (1), 5884−5903.

(6) Gajaria, T. K.; Chodvadiya, D.; Jha, P. K. Density Functional Theory Investigation of Thermal Conductivity in α-CN and α-CP Monolayers: Implications for Thermal Management of Electronic Devices. *ACS Appl. Nano Mater.* **2021**, *4*, 4474−4483.

(7) Sattigeri, R. M.; Gajaria, T. K.; Jha, P. K.; Spiewak, P.; Kurzydłowski, K. J. Emergence of s, p−d band inversion in zincblende gold iodide topological insulator and its thermoelectric properties. *J. Phys. Cond. Mater.* **2021**, *33*, 155402−155416.

(8) Hira, U.; Ali, S. S.; Latif, S.; Pryds, N.; Sher, F. Improved High-Temperature Thermoelectric Properties of Dual Doped $Ca_3Co_4O_9$. *ACS Omega* **2022**, *7*, 6579−6590.

(9) Shaabani, L.; Aminorroaya-Yamini, S.; Byrnes, J.; Akbar Nezhad, A.; Blake, G. R. Thermoelectric Performance of Na-Doped GeSe. *ACS Omega* **2017**, *2*, 9192−9198.

(10) Dwivedi, P.; Miyata, M.; Higashimine, K.; Takahashi, M.; Ohta, M.; Kubota, K.; Takida, H.; Akatsuka, T.; Maenosono, S. Nanobulk Thermoelectric Materials Fabricated from Chemically Synthesized $Cu_3Zn_{1x}Al_xSnS_{5y}$ Nanocrystals. *ACS Omega* **2019**, *4*, 16402−16408.

(11) Paudel, T. R.; Tsymbal, E. Y. Evaluating the Thermoelectric Properties of $BaTiS_3$ by Density Functional Theory. *ACS Omega* **2020**, *5*, 12385−12390.

(12) Zhu, L.; Jiang, X.; Gao, G.; Fu, H.; Yao, K. First-Principles Study on the Thermoelectric Properties of FeAsS. *ACS Omega* **2018**, *3*, 13630−13635.

(13) Tavares, S.; Yang, K.; Meyers, M. A. Heusler Alloys: Past, Properties, and Prospects. *Prog. Mater. Sci.* **2023**, *132*, 101017−101086.

(14) de Groot, R. A.; Mueller, F. M.; Engen, P. G. v.; Buschow, K. H. J. New Class of Materials: Half Metallic Ferromagnets. *Phys. Rev. Lett.* **1983**, *50*, 2024−2027.

(15) Nanda, R. K. B.; Dasgupta, I. Electronic structure and magnetism in half-Heusler compounds. *J. Phys.: Condens. Matter* **2003**, *15*, 7307−7323.

(16) Kalita, D.; Ram, M.; Limbu, N.; Kalita, R.; Saxena, A. Prediction of some physical properties in new half-Heusler alloy NbAgSi. *J. Solid State. Chem.* **2022**, *310*, 122999−123011.

(17) Joshi, H.; Rai, D. P.; Laref, A.; Thapa, R. K. Electronic, and thermoelectric properties of half-heusler compounds MCoSb (M = Ti, Zr, Hf): a first principles study. *Mater. Res. Exp.* **2019**, *06* (06), 066307−066326.

(18) Sofi, S. A.; Gupta, D. C. Pursuit of thermoelectric properties in $L2_1$ structured Co_2PAl (P = *Ru, Rh*) ductile ferromagnetic materials: A first principles prospective. *J. Solid State Chem.* **2021**, *296* (06), 121942−121950.

(19) Roy, A.; Bennett, J. W.; Rabe, K. M.; Vanderbilt, D. Half-Heusler Semiconductors as Piezoelectrics. *Phys. Rev. Lett.* **2012**, *109*, 037602−037606.

(20) Sootsman, J. R.; Chung, D. Y.; Kanatzidis, M. G. New and Old Concepts in Thermoelectric Materials. *Angew. Chem., Int. Ed.* **2009**, *48*, 8616−8639.

(21) Kawasaki, J. K.; Chatterjee, S.; Canfield, P. C. Full and half-Heusler compounds. *MRS Bull.* **2022**, *47*, 555−558.

(22) Chadov, S.; Qi, X.; Kübler, J.; Fecher, G. H.; Felser, C.; Zhang, S. C. Tunable multifunctional topological insulators in ternary Heusler compounds. *Nat. Mater.* **2010**, *9*, 541−545.

(23) Yadav, M. K.; Sanyal, B. First principles study of thermoelectric properties of Li-based half-Heusler alloys. *J. Alloys Compd.* **2015**, *622*, 388−393.

(24) Bhat, T. M.; Gupta, D. C. Analysis of electronic, thermal, and thermoelectric properties of the half-Heusler CrTiSi material using density functional theory. *J. Phys. Chem. Solids* **2018**, *119*, 281−287.

(25) Afaq, A.; Maaz, H.; Bakar, A.; Jamil, M. I. Reststrahlen Band Studies of RuCrX (X= Si, Ge, Sn) Half Heusler Alloys. *J. Elec. Mater.* **2019**, *48*, 5323−5327.

(26) Gupta, S. D.; Gupta, S. K.; Jha, P. K.; Ovsyuk, N. N. A first principles lattice dynamics and Raman spectra of the ferroelastic rutile to $CaCl_2$ phase transition in SnO_2 at high pressure. *J. Raman Spectrosc.* **2013**, *44*, 926−933.

(27) Jha, P. K.; Sanyal, S. P. Lattice vibrational properties of uranium chalcogenides. *Phys. B* **1995**, *216*, 125−131.

(28) Jha, P. K.; Sanyal, S. P. Phonon spectrum and lattice specific heat of the $HgBa_2CuO_4$ high-temperature superconductor. *Phys. C* **1996**, *271*, 6−10.

(29) Bakar, A.; Afaq, A.; Shoaib, M.; Dahshan, A.; Asif, M. Ab-initio study for the elastic stability, mechanical, electronic and optical properties of RuCrX (X= Si, Ge, Sn) half-Heusler alloys. *Phys. Scr.* **2022**, *97*, 075801−075813.

(30) Reshak, A. H.; Alahmed, Z. A.; Bila, J.; Atuchin, V. V.; Bazarov, B. G.; Prosvirin, O. O.; Molokeev, M. S.; Prosvirin, I. P.; Yelisseyev, A. P. Exploration of the Electronic Structure of Monoclinic α-

$Eu_2(MoO_4)_3$: DFT-Based Study and X-ray Photoelectron Spectroscopy. *J. Phys. Chem. C* **2016**, *120*, 10559−10568.
(31) Benaadad, M.; Nafidi, A.; Melkoud, S.; Khan, M. S.; Soubane, D. First-principles investigations of structural, optoelectronic and thermoelectric properties of Cu-based chalcogenides compounds. *J. Mater. Sci.* **2021**, *56*, 15882−15897.
(32) Khan, M. S.; Alshahrani, T.; Haq, B. U.; Azam, S.; Khan, G.; Alrobei, H.; Abbas, Z.; Predota, M.; Khan, M. A.; Benaadad, M. Investigation of structural, electronic and optical properties of potassium and lithium based ternary Selenoindate: Using first principles approach. *J. Solid State Chem.* **2021**, *293*, 121778−121788.
(33) Perdew, J. P.; Burke, K.; Ernzerhof, M. Generalized Gradient Approximation Made Simple. *Phys. Rev. Lett.* **1996**, *77*, 3865−3868.
(34) Giannozzi, P.; Baroni, S.; Bonini, N.; Calandra, M.; Car, R.; Cavazzoni, C.; Ceresoli, D.; Chiarotti, G. L.; Cococcioni, M.; Dabo, I.; et al. QUANTUM ESPRESSO: a modular and open-source software project for quantum simulations of materials. *J. Phys.: Condens. Matter* **2009**, *21*, 395502−395520.
(35) Monkhorst, H. J.; Pack, J. D. Special points for Brillouin-zone integrations. *Phys. Rev. B* **1976**, *13*, 5188−5192.
(36) Madsen, G. K.H.; Singh, D. J. BoltzTraP. A code for calculating band-structure dependent quantities. *Comput. Phys. Commun.* **2006**, *175*, 67−71.
(37) Saini, A.; Singh, R.; AlShaikhi, A. A.; Kumar, R. Effect of temperature dependent relaxation time of charge carriers on the thermoelectric properties of LiScX (X = C, Si, Ge) half-Heusler alloys. *J. Alloy. Comp.* **2019**, *806*, 1536−1541.
(38) Singh, D. J. Doping-dependent thermopower of PbTe from Boltzmann transport calculations. *Phys. Rev. B* **2010**, *81*, 195217−195222.
(39) Wang, D.; Wang, D. Electronic structure and thermoelectric properties of Pb-based half-Heusler compounds: ABPb (A = Hf, Zr; B = Ni, Pd). *J. Alloy. Comp.* **2016**, *682*, 375−380.
(40) Guo, S. D. Thermoelectric properties of half-Heusler ZrNiPb by using first principles calculations. *RSC Adv.* **2016**, *6* (53), 47953−47958.
(41) Li, W.; Yang, G.; Zhang, J. Optimization of the thermoelectric properties of FeNbSb-based half-Heusler materials. *J. Phys. D Appl. Phys.* **2016**, *49* (19), 195601−195605.
(42) Ong, K. P.; Singh, D. J.; Wu, P. Analysis of the thermoelectric properties of n-type ZnO. *Phys. Rev. B* **2011**, *11*, 115110−115114.
(43) Ali, Z.; Ahmad, I.; Khan, I.; Amin, B. Electronic structure of cubic perovskite $SnTaO_3$. *Intermetallics* **2012**, *31*, 287−291.
(44) Kim, C.; Pilania, G.; Ramprasad, R. Machine Learning Assisted Predictions of Intrinsic Dielectric Breakdown Strength of ABX_3 Perovskites. *J. Phys. Chem. C* **2016**, *120*, 14575−14580.
(45) Wolpert, D., Ampadu, P., Eds.; *Managing Temperature Effects in Nanoscale Adaptive Systems*, 3rd ed.; Springer: New York, 2012; pp 1−13.

https://doi.org/10.1021/acsomega.2c05928
ACS Omega 2022, 7, 45353−45360